Asian Herpetological Research 2017, 8(4): 235–243
DOI: 10.16373/j.cnki.ahr.170069

ORIGINAL ARTICLE

Nondestructive Skeletal Imaging of *Hyla suweonensis* Using Micro-Computed Tomography

Eunbin KIM[1], Hacheol SUNG[2], Donghyun LEE[2], Geunjoong KIM[2], Dongha NAM[2*] and Eungsam KIM[2*]

[1] *School of Biological Sciences and Biotechnology, Chonnam National University, 77, Yongbong-ro, Bukgu, Gwangju* 61186, *South Korea*

[2] *Department of Biological Sciences, College of Natural Sciences, Chonnam National University, 77, Yongbong-ro, Bukgu, Gwangju* 61186, *South Korea*

Abstract We successfully obtained 3D skeletal images of *Hyla suweonensis*, employing a nondestructive method by applying appropriate anesthesia and limiting the radiation dose. *H. suweonensis* is a tree frog endemic to Korea and is on the list of endangered species. Previous studies have employed caliper-based measurements and two-dimensional (2D) X-ray imaging for anatomical analyses of the skeletal system or bone types of *H. suweonensis*. In this work we reconstructed three-dimensional (3D) skeletal images of *H. suweonensis*, utilizing a nondestructive micro-computed tomography (micro-CT) with a short scan and low radiation dose (i.e. 4 min and 0.16 Gy). Importantly, our approach can be applied to the imaging of 3D skeletal systems of other endangered frog species, allowing both versatile and high contrast images of anatomical structures without causing any significant damages to the living animal.

Keywords *Hyla suweonensis*, Micro-computed tomography, 3D skeletal structure, Nondestructive imaging, Endangered species, Radiation dose.

1. Introduction

The genus *Hyla* is a member of the family of tree frogs (Hylidae), which is widely distributed across North America, Africa, and Eurasia (Faivovich *et al.*, 2005). *Hyla suweonensis* that is endemic to Korea and critically endangered has decreased to 800 individuals (reported from International Union for Conservation of Nature, 2017). Since the first description of *H. suweonensis* that distinguished it from other members of the *Hyla* genus, based on its morphological and call variations (Kuramoto, 1980), *H. suweonensis* has been reported in Korea (Borzée and Jang, 2015; Kim *et al.*, 2012a; Kim *et al.*, 2012b) and its phylogenetic relationships have been conducted based on full mitochondrial DNA sequences, recently (Borzée *et al.*, 2017; Lee *et al.*, 2017; Nam *et al.*, 2017). However, discriminating *H. suweonensis* and *H. japonica*, the sibling species, is still a challenge due to their similar morphologies, and the limited information on their osteological features (Borzée *et al.*, 2013; Suh *et al.*, 1996; Yang *et al.*, 1981; Yang and Park, 1988).

Osteology is important for understanding both the external and internal morphology of animal. More importantly, such key features allow us to identify frog species and to study systematics, phylogenetics, morphological and behavioral evolution of frogs. (Zug, 1972; Zug, 1978; Reilly and Jorgensen, 2011; Jorgensen and Reilly, 2013; Klages *et al.*, 2013; Scherz *et al.*, 2016; Zhang *et al.*, 2016). Although dissection techniques have provided vital information on the skeleton and osteological characteristics, these conventional procedures are destructive. Dissection, in turn, prevents the damaged

* Corresponding author: Dr. Dongha NAM, from Chonnam National University, Gwangju, South Korea, with his research focusing on conservation biology and ecotoxicology; Dr. Eungsam KIM, from Chonnam National University, Gwangju, South Korea, with his research focusing on cell mechanobiology and nanobiosystems.
E-mail: dongha@chonnam.ac.kr (Dongha NAM); eungsam.kim@chonnam.ac.kr (Eungsam KIM)
Received: 5 September 2017 Accepted: 29 November 2017

specimen from being used for further investigations, which would require the same specimen to be intact.

Recently, micro-computed tomography (micro-CT) has been used not only in biomedical imaging studies but also in zoological research (Klages *et al.*, 2013; Krings *et al.*, 2017; Scherz *et al.*, 2016). The CT scanning approach combining X-ray irradiation and image-processing algorithm produces tomographic images of specific regions of a scanned specimen from different angles, which thereby allows researchers to examine the inner parts of the biological specimen without surgical dissection, while conventional X-ray-based imaging provides 2D images that can give limited information. Moreover, the intact sample after micro-CT imaging can be subjected to further investigations relating any approaches, resolving the issue of having insufficient specimen samples. Similarly, micro-CT is currently being employed in ecological applications, in order to assess the relationship between ecological conditions and morphological skeletal features of living organisms (Krings *et al.*, 2017).

This work aims to visualize detailed architectures of the skeletal system of *H. suweonensis* alive, using nondestructive micro-CT. These 3D skeletal data will contribute to more accurate identification of the species and its morphometric analysis, which are essential for conservation of this globally threatened species.

2. Materials and Methods

2.1 Sampling and management of *H. suweonensis* All aspects of this study were approved by the Chonnam National University Animal Care and Use Committee. The ten specimens of *H. suweonensis* were collected at Iksan (35°58'45.3" N, 126°55'09.7" E; datum WGS 84) between May and June in 2016, with permission from the Saemangeum Regional Environment Management Office that is in charge of the conservation of endangered species in Jeollabuk-do, Korea. The specimens were sampled from rice paddies, which provided temporary wetland habitats during their breeding season. We tracked the advertisement calls of *H. suweonensis* and collected them at the sampling sites during nighttime (between 5 p.m. to 3 a.m.). Only male frogs were sampled on the basis of their advertisement call. We also sampled *H. japonica* at the same site where the *H. suweonensis* was collected to identify these sympatric species.

Captured frogs were individually placed in a 32 cm (L) × 19 cm (D) × 24 cm (H) size terrarium with a 5 cm-thick sterilized coco peat, and an assortment of plastic bowls containing fresh water and food. The temperature, humidity and light conditions of the terrarium were controlled to mimic those of the frog habitat.

2.2 Species confirmation To verify whether the collected frogs were *H. suweonensis*, the morphological and vocal features of each frog were analyzed. We took images of the specimen by placing them parallel to the plane of the lens of the camera in order to acquire direct measurements of the angles and shapes of the frog head; we measured the angles between the two lines from the eyes to nostrils using ImageJ (ver. 1.50, National Institutes of Health, Bethesda, MD, USA) (Borzée *et al.*, 2013). All photographs were taken with a scale bar as a reference for morphometric measurement. Frog vocalization was recorded in captivity using an action camera (SJ4000, SJCAM, China). Advertisement calls of *H. suweonensis* and *H. japonica* were analyzed by Raven (version pro 1.5, Cornell Laboratory of Ornithology, USA) (Park *et al.*, 2013), with a 100 sample Fast Fourier Transform and a Hann smoothing window, resulting in a temporal resolution of 1 ms and a frequency resolution of 32.8 Hz. Sound oscillograms were made after filtering around 500 – 4 000 Hz to inspect the pulse pattern.

2.3 Inhalational anesthesia Prior to micro-CT scanning, each frog was placed in an anesthesia system (XGI-8 Gas Anesthesia System, Perkin Elmer, USA), containing a 4% isoflurane/oxygen gas mixture (ISOTROY 100, Troikaa, India), for 10 to 40 min. Anesthesia was confirmed by observing that the eyes of the frog was closed and it no longer responded to external stimuli. To maintain the anesthetic state of the frog during the scanning process, the concentration of the inhalational anesthetic was kept at 4% within the micro-CT equipment. We used five frogs to set up our experiment to determine isoflurane concentration. Following the micro-CT scan, the frog was placed in a glass tank with wet gauze to allow for recovery from the anesthesia. The recovery time was defined as the time point when the frog was awakened from the anesthetic state to open eyes and presented jumping, climbing (walking on the wall), and feeding.

2.4 Micro-CT scanning Micro-CT imaging was performed using a Quantum GX μCT imaging system (PerkinElmer, Waltham, MA, USA), located at Korea Basic Science Institute (Gwangju, Korea). A 3D micro-CT scanning system equipped with an X-ray tube (voltage 90 kV, current 88 μA) was applied to visualize the skeleton of the frog in a set-up with a voxel size of 90 μm, field of view (FOV) of 45 mm × 45 mm, working distance of 108 mm, and scan time of 4 min in high resolution scan mode

for the whole body; and a voxel size of 50 μm, FOV of 25 mm × 25 mm, working distance of 55 mm, and scan time of 2 min was employed in standard scan mode for the skull, manus and pes. Skeleton images were taken from the two specimens.

The radiation doses of the micro-CT scan were 0.16 Gy for the whole body and 1.48 Gy for the head, manus and pes since they were determined by setting parameters above. The anesthetized frog was placed on an acrylic plate attached to an animal bed in micro-CT. Its forelimbs and hindlimbs were carefully stretched, and then the head, body and joints of the frog were pressed down slightly to adhere to the acrylic plate for measurement of bone length on micro-CT image. Manus and pes digits were stretched using a blunt end tweezer to avoid their overlapping. We spread a little water on the dorsum to prevent the frog from drying during the micro-CT scan. As a reference scale bar, a 1 cm-long bone of a mouse was placed adjacent to the frog.

2.5 Reconstruction of 3D images The scanned data were reconstructed to obtain 3D skeletal images (JPG format) and movies (AVI format) with a micro-CT viewer and 3D viewer programs, which were both provided by PerkinElmer. Subvolume reconstruction is a function of the software that allows the researcher to obtain fine images of specific body regions by generating higher resolution reconstructions of areas of interest without the need to re-scan the sample. We performed subvolume reconstructions of the head, manus and pes from the whole-body scan data to acquire fine images without submitting the animals to additional X-ray irradiation. The terminology for osteology follows Trueb's notation (Trueb, 1973; Trueb, 1993).

3. Results

3.1 Morphological features and call structures of *H. suweonensis* The color of the dorsal sides of the head and limbs of a male frog with its weight of 2.0 g was green (Figure 1A). There were dark brown bands extending from the eye to the tympanum. Additionally, dark brown spots were found near the tympanum through the lateral sides on the frog. The ventral side of the abdomen was whitish but the ventral side of the thigh was yellowish. The surface of the abdomen, ventral side of forelimbs and hindlimbs was covered with tiny bumps. The colors of the pupil and iris were black and gold, respectively. The vocal sac was yellowish. The angle between the two lines connecting the anterior corners of the eyes and the ipsilateral nostrils was 72.6° (Figure 1B). The angle between the two lines connecting the posterior corners of the eyes and the ipsilateral nostrils was 64.6°. The first, second, fifth, third and fourth toes from the proximal body were listed in order of length. The third and fifth toes showed similar lengths.

We recorded one call bout with 11 notes of the *H. suweonensis* and one call bout with 28 notes of the *H. japonica* in a terrarium (audio files of the advertisement call of the two frogs are available in Supplementary Materials). The note duration and note period of the *H. suweonensis* calls was 0.17 ± 0.03 s and 0.33 ± 0.09 s, respectively, in average (Figure 1C). We could identify call characteristics of the *H. suweonensis* with high amplitude modulation in the beginning part of each note and some connected pulses, which accounts for higher frequencies sounds in the spectrum compared with those of *H. japonica*. The note duration and note period of the call of *H. japonica* was 0.12 ± 0.03 s and 0.17 ± 0.01 s, respectively (Figure S1). Furthermore, sound oscillograms showed typical pulse patterns with no connected pulses of *H. japonica* calls (Park *et al.*, 2013). Accordingly, our specimen demonstrated the typical traits of *H. suweonensis*, based on morphometric (e.g., head angles and toe-structure arrangement) and advertisement call (e.g. high amplitude modulation and connected pulses) characteristics compared to its sibling species, *H. japonica* (Borzée *et al.*, 2013; Park *et al.*, 2013).

3.2 Osteology of *H. suweonensis* Using an identified frog as a model, we present 3D skeletal images of the globally endangered species, *H. suweonensis* (Figure 2; 3D movies for the entire skeleton, skull, manus and pes are available in Supplementary Materials). The entire skeleton of *H. suweonensis* was 32 mm in length along the anterior-posterior axis, exhibiting bilateral symmetry (Figures 2 and 3A). The vertebrae of the spine consisted of seven vertebral segments with an incomplete separation of the two uppermost segments. The humerus was longer than the radio-ulna in the forelimb: 7.8 mm (humerus) versus 5.7 mm (radio-ulna). The proximal end of the humerus was slightly broader than its distal end. The hindlimb was composed of three types of bones: femur, tibiofibula, and tarsus. The femur and tibiofibula were almost the same length at 13.4 mm. The length of the tarsus was 8.2 mm. The urostyle had a well-developed dorsal ridge along its dorsal side. Some frogs have iliac shafts with deep oblique grooves of a rounded shape (Lambert *et al.*, 2017), whereas the iliac shafts bore a linear form with a V-shaped contour in the *H. suweonensis*. The distal ends of the sacrum were flat and wide, like a bowtie with a curved bony margin.

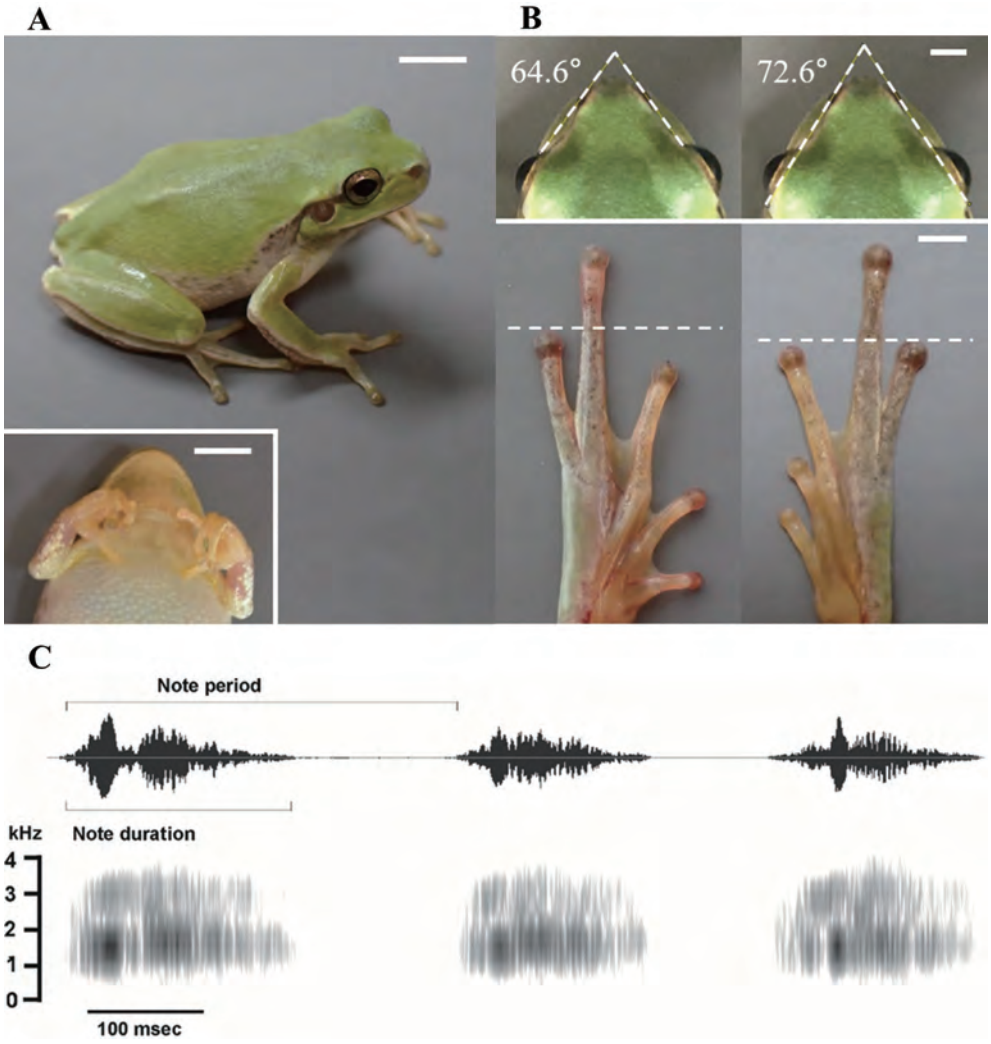

Figure 1 Validation of the morphological and call features of *Hyla suweonensis*. A: dorsolateral view of the adult male (inset: ventral view of the frog) (body weight: 2.0 g); B: dorsal view of the frog with angle measurements, dorsal view of the left and right pes; C: oscillogram and sound spectrogram of the advertisement call. Scale bars: 5 mm (A) and 2 mm (B).

The free ends of the two clavicles were bent toward the skull and slightly contacted to each other, whereas a pair of coracoids were spaced 1 mm apart (Figure 3B). The ossified posteromedial processes (pmp) were located between the clavicles and the skull. The first and second diapophyses bent towards the ventral side, while the other diapophyses straightly extended to the lateral side (Figure 3C). The terminal end of the urostyle was separated from the ilium.

The semi-ellipse-shaped skull had a basal width of about 11 mm from the dorsal side and a central height of about 9.4 mm from the ventral side (Figure 3D and 3E). The nasal bones (nas) were paired, elongated anteroposteriorly. The neopalatines (npl) were connected to the sphenethmoid (spheth) and the maxillary. The sphenethmoid bone (spheth) covered the dorsal and lateral sides of the brain case anteriorly, but made no contact with the nasal bone. The frontoparietal (fpar) was composed of thin bones, which formed compartments that incompletely covered the brain. The prootics (pro) were either fused with or contacted to the exoccipitals (exocc), composing the posterior portion of the skull. The pterygoid (pter) bone was a triradiate structure located in the posteroventral region of the skull. The prevomers (pvom) consisted of a large odontophore overlapping with the sphenethmoid bone in the ventral side. The dentary (dent) was narrow, curved anteriorly and fused with the rod-shaped mentomeckelian (mmk) bones. The main bone of the jaw was a long angular (ang) bone, which was separated from the mentomeckelian bone. The alary process of the premaxillary (al.proc) was protruded at 60° to the horizontal line from the lateral view (Figure 3F).

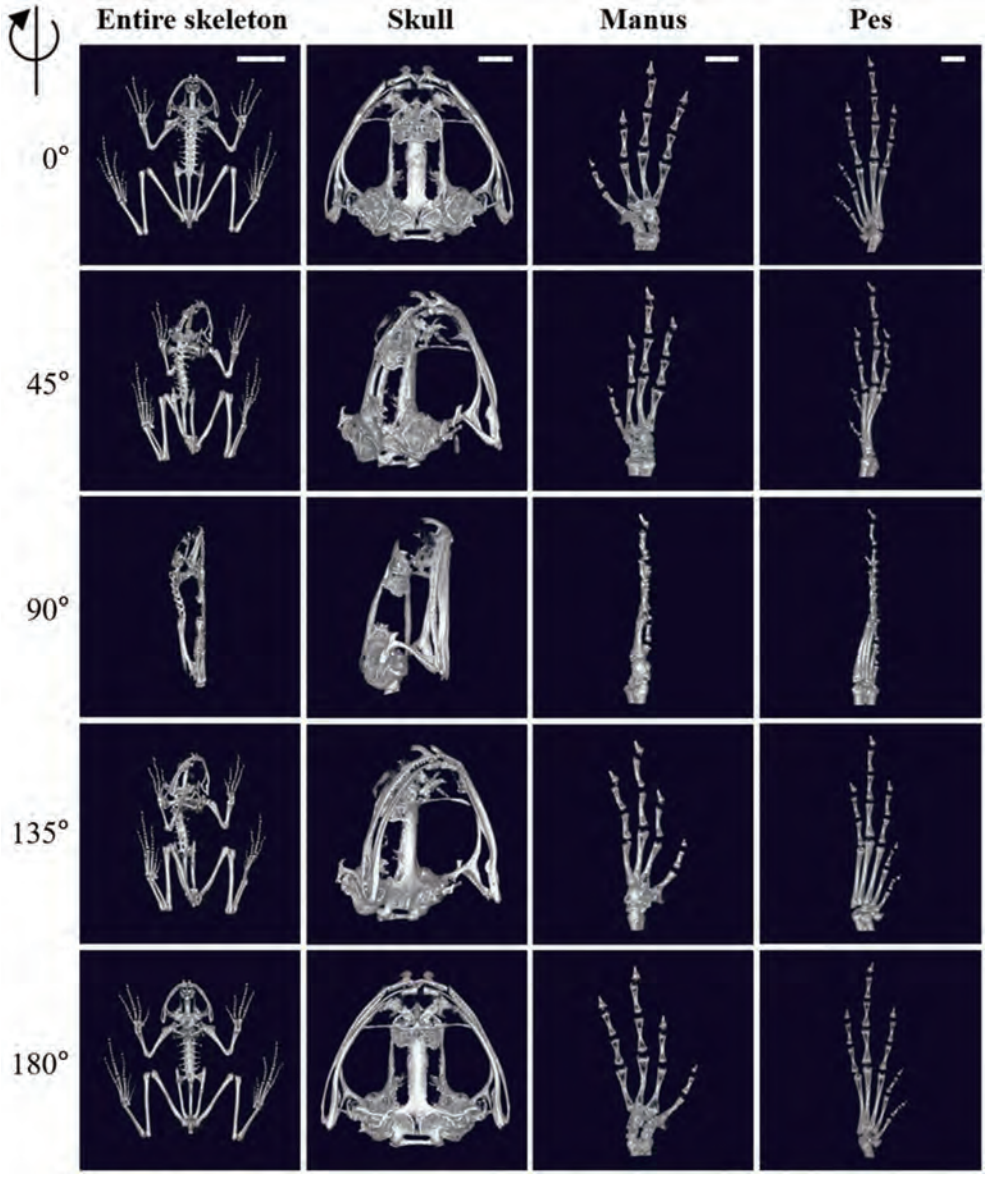

Figure 2 Still images from the 3D micro-CT movies of *Hyla suweonensis*. The static images were captured from the 3D movie of the entire skeleton, skull, right manus, and right pes at the angle (0, 45, 90, 135, and 180 degrees clockwise around the central axis). Scale bars: 10 mm (entire skeleton) and 2 mm (skull, manus, and pes).

The tripod-shaped septomaxillaries (spmax) were paired, and located between the nasal and prevomer bones. The squamosal (sq) was T-shaped.

The terminal phalanges in all the digits were sharp and conical in shape like an arrowhead (Figure 2). The phalangeal formulas to represent the numbers of digital bones were 2-2-3-3 and 2-2-3-4-3 for the manus and pes, respectively (Figure 3G and 3H). The gap between the two neighboring phalangeal bones in the manus and pes was 0.3 mm in length. The prepollex and prehallux both projected laterally were also observed in the manus and pes though they were small.

4. Discussion

4.1 Minimizing chemical and radiation damages to frogs Following the identification of *H. suweonensis*, on the basis of its external morphology and acoustic characteristics (Figure 1), inhalational anesthesia was performed to restrict its movements in order to conduct a micro-CT scan. As isoflurane is widely used as an anesthetic in biomedical research (West *et al.*, 2014), the specimens were anesthetized with an isoflurane/air mixture (4% in 100% oxygen) for 10 to 40 min. The elapsed time from the onset of anesthesia to recovery

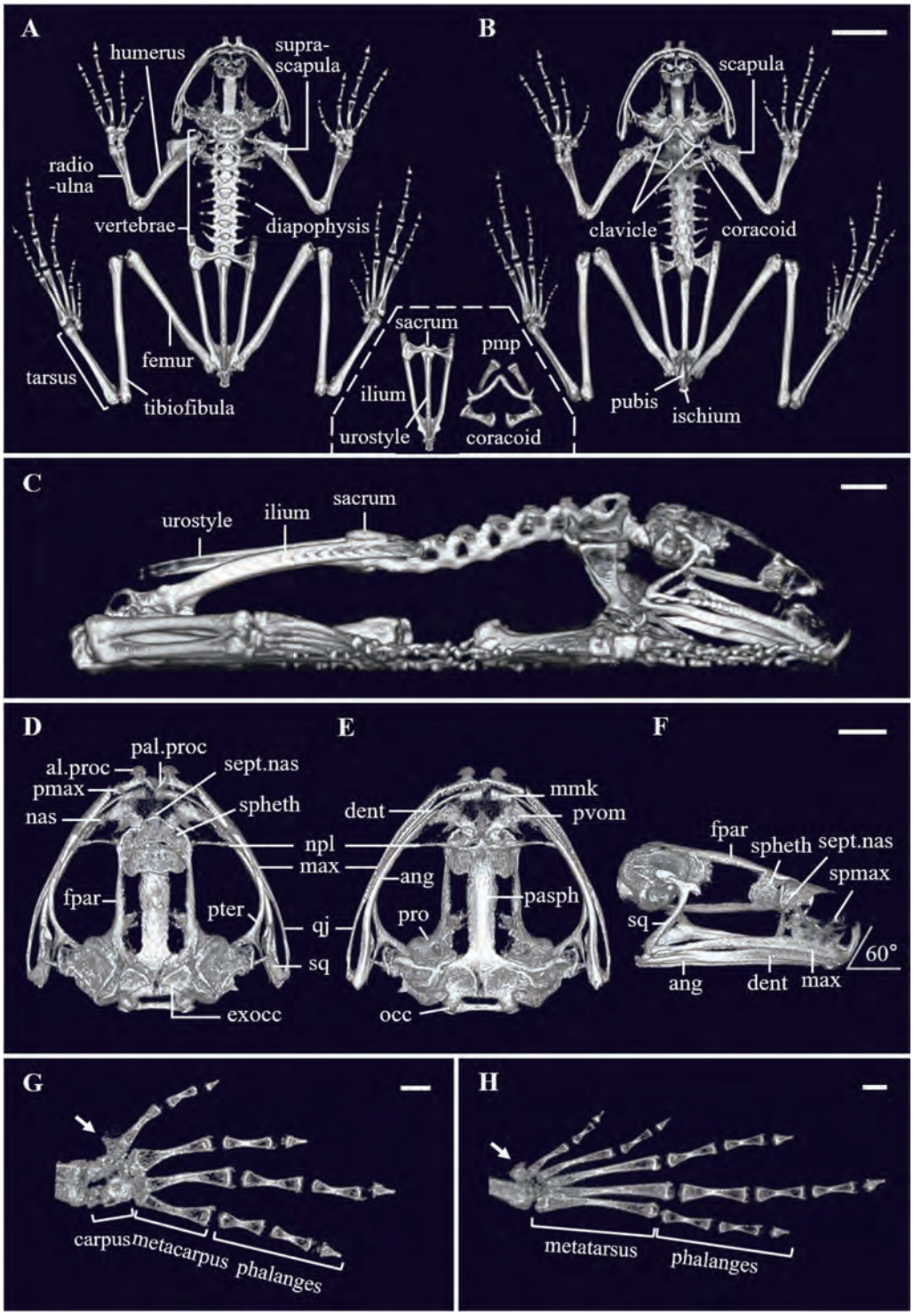

Figure 3 Three-dimensional micro-CT images of *Hyla suweonensis* by X-ray radiation dose of 0.16 Gy. A: entire skeleton, dorsal view, high resolution mode scan image; B: entire skeleton, ventral view, high resolution mode scan image (sacrum, ilium, urostyle, coracoid and posteromedial processes (pmp) were marked in the inset); C: entire skeleton, lateral view, high resolution mode scan image; D: skull, dorsal view, subvolume reconstruction image; E: skull, ventral view, subvolume reconstruction image; F: skull, lateral view, subvolume reconstruction image (abbreviations: al.proc, alary process of premaxillary; ang, angular; dent, dentary; exocc, exoccipital; fpar, frontoparietal; max, maxillary; mmk, mentomeckelian; nas, nasal; npl, neopalatine; occ, occipital condyle; pal.proc, palatine process; pasph, parasphenoid; pmx, premaxilla; pmp, posteromedial processes; pro, prootic; pter, pterygoid; pvom, prevomer; qj, quadratojugal; sept.nas, septum nasi; spheth, sphenethmoid; spmax, septomaxillary; sq, squamosal); G: right manus, dorsal view, subvolume reconstruction image (an arrow points to the prepollex); H: right pes, dorsal view, subvolume reconstruction image (an arrow points to the prehallux). Scale bars: 5 mm (A–B), 2 mm (C–F), and 1 mm (G–H).

reached up to 30 min (when the frog began demonstrating specific behaviors such as open his eyes and raise his head) and 3 h (demonstrating normal behaviors such as jumping, climbing, and feeding).

Previous studies have reported that radiation damages to frogs were mostly dependent on the dose of X-ray. For example, when *Rana pipiens* was irradiated at 10 Gy X-ray, erythrocytes swelled with abnormal nuclei and vacuoles in the cytoplasm of white blood cells increased in size (Lessler and Herrera, 1962). Correspondingly, a dislocation of the otoconia, reflecting damage from X-ray irradiation, occurred in *R. esculenta*, which had been irradiated with 1 500 Gy X-ray (Boistel *et al.*, 2009). The electrical capacitance was also shown to increase in 1 Gy X-ray irradiated bull frogs, which may be interpreted as physical evidence of changes in erythrocytes (Lessler, 1959). The genus *Amphiuma* of amphibians showed irregular erythrocytes cells when irradiated with 0.5 to 1 Gy X-ray (Lessler, 1959). We note that in this work, the X-ray radiation dose for the whole-body scan (at a setting with FOV of 45 mm × 45 mm, a scan time for 4 min at high resolution scan mode) was 0.16 Gy; and that of head, manus and pes scans (FOV of 25 mm × 25 mm and scan time of 2 min at standard scan mode) were approximately 1.48 Gy. We applied a higher X-ray dose of 2.95 Gy (FOV of 25 mm × 25 mm and scan time 4 min at the high resolution scan mode) to the manus and pes to investigate the effect of the radiation dose on the apparent quality of images (Figure S2G and S2H). Despite the fact that the skeletal images of the head, manus and pes provided higher resolution than the subvolume reconstruction images from the whole-body scan data (Figure 3D to 3H, Figure 4), the subvolume reconstruction images were adequate for verifying detailed skeletal structures of the scanned images without an additional X-ray radiation dose. For this reason, we believe that subvolume reconstruction images from the whole-body scan data (0.16 Gy) that require no additional radiation dose, compared to the aforementioned studies (0.5 – 1 500 Gy), are sufficient to observe primary bone structures, and that these approaches may help to minimize the health risk caused by irradiation, especially of endangered species. Nevertheless, repeated inhalational anesthesia and micro-CT scans are a general health concern for these specimens that should be substantiated on the basis of optimal experimental conditions (Broeckhoven *et al.*, 2017).

4.2 Micro-CT imaging of skeletal configuration of *H. suweonensis* As we reconstructed 3D skeletal images of *H. suweonensis* (Figures 2, 3, S2), we were able to observe its general characteristics such as the features of the vertebral column, phalangeal formula, shape of distal end of phalanges and Emerson's ilio-sacral articulation type of the frog. In addition, these data provided precise skeletal structures from various angles, which were not seen in 2D images. To the best of our knowledge, this study is the first report presenting 3D skeletal images of *H. suweonensis* (order Anura) that were obtained without having to sacrifice the animal.

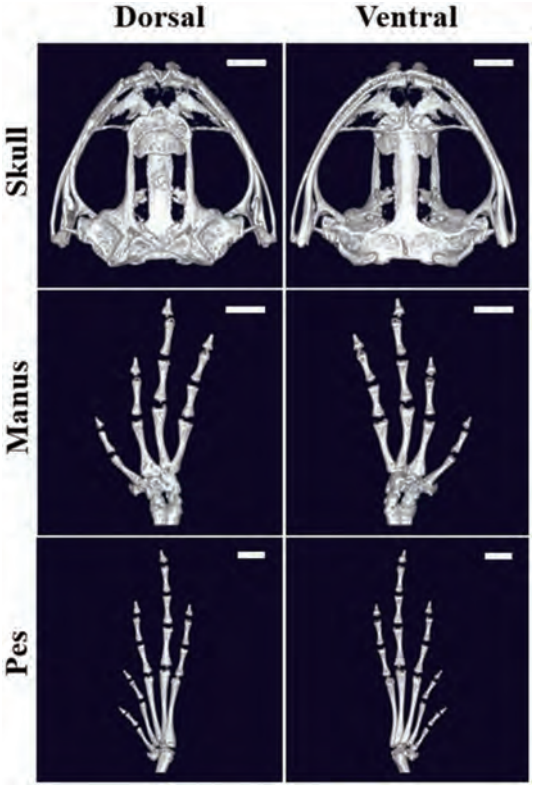

Figure 4 Micro-CT images of *Hyla suweonensis* by X-ray radiation dose of 1.48 Gy. Dorsal and ventral views of the skull, right manus, and right pes. Scale bars: 2 mm.

Collectively, *H. suweonensis* represents type IIA of Emerson's ilio-sacral articulations in anurans (Emerson, 1979; Reilly and Jorgensen, 2011). Although we were not permitted to dissect the specimen to observe its articulation type, these skeletal configurations with a lateral bent shape and extended pelvic systems (such as a bowtie-like sacrum with a curved bony margin) could reflect its function; thus, it may aid in specific locomotor activities via lateral rotation movement.

Previous studies on frogs have linked morphological skeletal characteristics to specific locomotor activities such as jumping, walking and other behaviors. For example, Emerson's ilio-sacral articulation type has relevance in walking speed, jumping distance and burrowing (Emerson, 1979). Of note, the hindlimb length,

sacral width, as well as the ratio length of the humerus to the tibiofibula, can be used to distinguish between the locomotor modes of frogs (Petrović *et al.*, 2017). In the future, utilizing a nondestructive methodology to visualize the skeletal system of *H. suweonensis* and other amphibians will provide more relevant information of the morphology and its relation to behavior and evolution.

5. Conclusion

Using a nondestructive method based on micro-CT, this work successfully reconstructed 3D skeletal images of *H. suweonensis*, a globally endangered species. This nondestructive approach will enable us to perform a longitudinal study of the tree frog; and correspondingly, not only to describe the skeletal systems of this animal, but also to uncover the relationship between its habitat use and its locomotor behavior.

Acknowledgements This research was supported by Basic Science Research Program through the National Research Foundation of Korea (NRF) funded by the Ministry of Science, ICT and Future Planning (grant numbers: NRF-2015R1C1A1A01052498 and NRF-2014R1A1A1006010). We are grateful to Dr. Jaeil PARK (Korea Basic Science Institute) for conducting the *in vivo* micro-CT analyses. Our special thanks go to Choongho HAM, Donggwon KIM, Hyunah LEE and Amir Roshanzadeh for the management and collection of the samples as well as the edition of movie file.

References

Boistel R., Pollet N., Tinevez J. Y., Cloetens P., Schlenker M. 2009. Irradiation damage to frog inner ear during synchrotron radiation tomographic investigation. J Electron Spectrosc, 170(1): 37–41

Borzée A., Didinger C., Jang Y. K. 2017. Complete mitochondrial genome of *Dryophytes suweonensis* (Anura Hylidae). Mitochondr DNA Part B, 2(1): 5–6

Borzée A., Jang Y. K. 2015. Description of a seminatural habitat of the endangered Suweon treefrog *Hyla suweonensis*. Anim Cells Syst, 19(3): 216–220

Borzée A., Park S. Y., Kim A. B., Kim H. T., Jang Y. K. 2013. Morphometrics of two sympatric species of tree frogs in Korea: a morphological key for the critically endangered *Hyla suweonensis* in relation to *H. japonica*. Anim Cells Syst, 17(5): 348–356

Broeckhoven C., Plessis A., Roux S. G., Mouton P. L. F. N., Hui C. 2017. Beauty is more than skin deep: a non-invasive protocol for in vivo anatomical study using micro-CT. Methods Ecol Evol, 8(3): 358–369

Emerson S. B. 1979. The ilio-sacral articulation in frogs: form and function. Biol J Linn Soc, 11(2): 153–168

Faivovich J., Haddad C. F., Garcia P. C., Frost D. R., Campbell J. A.,Wheeler W. C. 2005. Systematic review of the frog family Hylidae, with special reference to Hylinae: phylogenetic analysis and taxonomic revision. B Am Mus Nat Hist, 1–240

IUCN (International Union for Conservation of Nature). 2017. Internet references. http://www.iucnredlist.org/details/55670/0

Jorgensen M., Reilly S. 2013. Phylogenetic patterns of skeletal morphometrics and pelvic traits in relation to locomotor mode in frogs. J Evolution Biol, 26(5): 929–943

Kim I. H., Ham C. H., Jang S. W., Kim E. Y., Kim J. B. 2012a. Determination of breeding season, and daily pattern of calling behavior of the endangered Suweon-tree frog (*Hyla suweonensis*). Korean J Herpetol, 4: 23–29 (In Korean with English abstract)

Kim I. H., Son S. H., Kang S. W., Kim J. B. 2012b. Distribution and habitat characteristics of the endangered Suweon-tree frog (*Hyla suweonensis*). Korean J of Herpetol, 4: 15–22 (In Korean with English abstract)

Klages J., Glaw F., Köhler J., Müller J., Hipsley C. A., Vences M. 2013. Molecular, morphological and osteological differentiation of a new species of microhylid frog of the genus *Stumpffia* from northwestern Madagascar. Zootaxa, 3717(2): 280–300

Krings M., Klein B., Heneka M. J., Rödder D. 2017. Morphological comparison of five species of poison dart frogs of the genus *Ranitomeya* (Anura: Dendrobatidae) including the skeleton, the muscle system and inner organs. PLOS ONE, 12(2): e0171669

Kuramoto M. 1980. Mating calls of treefrogs (genus *Hyla*) in the Far East, with description of a new species from Korea. Copeia, 100–108

Lambert S. M., Hutter C. R., Scherz M. D. 2017. Diamond in the rough: a new species of fossorial diamond frog (*Rhombophryne*) from Ranomafana National Park, southeastern Madagascar. Zoosyst Evol, 93: 143

Lee M. Y., Jeon H. S., Min M. S., An J. H. 2017. Sequencing and analysis of the complete mitochondrial genome of *Hyla suweonensis* (Anura: Hylidae). Mitochondr DNA Part B, 2(1): 126–127

Lessler M. A. 1959. Low-level X-ray damage to amphibian erythrocytes. Science, 129(3362): 1551–1553

Lessler M. A., Herrera F. M. 1962. Electron-microscope studies of x-ray damage to frog blood cells. Radiat Res, 17(2): 111–117

Nam D. H., Lee H. A., Kim E. B., Kim G. J., Kim E. S., Park C. G., Sung H. C., Lee D. H. 2017. Complete mitochondrial genome of a treefrog, *Hyla* sp.(Anura: Hylidae). Mitochondr DNA Part B, 2(1): 221–222

Park S. Y., Jeong G. S., Jang Y. K. 2013. No reproductive character displacement in male advertisement signals of *Hyla japonica* in relation to the sympatric *H. suweonensis*. Behav Ecol Sociobiol, 67(8): 1345–1355

Petrović T. G., Vukov T. D., Tomašević Kolarov N. 2017. Morphometric ratio analyses: Locomotor mode in anurans. C R Biol, 340(4): 250–257

Reilly S. M., Jorgensen M. E. 2011. The evolution of jumping in frogs: morphological evidence for the basal anuran locomotor condition and the radiation of locomotor systems in crown group anurans. J Morphol, 272(2): 149–168

Scherz M. D., Vences M., Rakotoarison A., Andreone F.,

Köhler J., Glaw F., Crottini A. 2016. Reconciling molecular phylogeny, morphological divergence and classification of Madagascan narrow-mouthed frogs (Amphibia: Microhylidae). Mol Phylogenet Evol, 100: 372–381

Suh J. H., Kim J. B., Min M. S., Suk H. Y., Yang S. Y. 1996. Skeletal character variation of 2 species of the genus *Hyla*. Bull Inst Basic Sci Inha Univ, 17: 41–50 (In Korean with English abstract)

Trube L. 1973. Evolutionary biology of the anurans: contemporary research on major problems. Columbia, USA: University of Missouri Press. 65–132 pp

Trube L. 1993. The Skull, Volume 2: Patterns of Structural and Systematic Diversity. Chicago, USA: The University of Chicago Press. 255–343 pp

West G., Heard D., Caulkett N. 2014. Zoo animal and wildlife immobilization and anesthesia. Hoboken, USA: John Wiley and Sons. 308 pp

Yang S. Y., Park B. S. 1988. Speciation of the two species of the genus *Hyla* (anura) in Korea. Korean J Zool, 31: 11–20 (In Korean)

Yang S. Y., Park B. S., Son H. J. 1981. Species comparison of the genus *Hyla* in Korea. Bull Inst Basic Sci Inha Univ, 2: 75–83 (In Korean with English abstract)

Zhang M., Xiaoping C., Xiaohong C. 2016. Osteology of *Quasipaa robertingeri* (Anura: Dicroglossidae). Asian Herpetol Res, 7(4): 242–250

Zug G. R. 1972. Anuran locomotion: Structure and function. I. Preliminary observations on relation between jumping and osteometrics of appendicular and postaxial skeleton. Copeia, 613–624

Zug G. R. 1978. Anuran locomotion-structure and function: Jumping performance of semiaquatic, terrestrial, and arboreal frogs. Smithsonian Institution Press. 1–21 pp

Supplementary Materials

The oscillogram and sound spectrogram of the advertisement call of *H. japonica* were obtained using the same method for those of *H. suweonensis* as described in Materials and Methods. The 0.7 second-long profile as below shows a part the whole call recorded for 8 s (Figure S1).

Audio files for advertisement calls of two tree frogs. (Audio file 1) Advertisement calls of *H. suweonensis*. (Audio file 2) Advertisement calls of *H. japonica* (https://pan.baidu.com/s/1sln2i4l).

These files with the AVI format contain 8-second-long advertisement calls of *H. suweonensis* and *H. japonica*. Each frog was placed in a 32 cm (L) × 19 cm (D) × 24 cm (H) size terrarium under the same condition of light, humidity and temperature. Advertisement calls were recorded in the nighttime from 7 pm to 6 am when they croaked. The advertisement call of *H. suweonensis* has a longer note duration and note period as well as higher frequencies compared to that of *H. japonica*.

3D micro-CT movies of the skeleton of *H. suweonensis*. (Movie 1) Entire skeleton. (Movie2) Skull. (Movie 3) Manus. (Movie 4) Pes. (https://pan.baidu.com/s/1o7VXpGI).

These AVI-formatted files are 3D skeletal movies of *H. suweonensis* reconstructed via micro-CT viewer and 3D viewer programs both provided by PerkinElmer. The skeletal image rotates 360 degrees around the anterior-posterior axis during the period of 30 s. The entire skeleton movie was obtained from the high resolution scan mode of a 4-minuate-long micro-CT scan data. Other movies were obtained by the sub-volume reconstruction applied to whole body scan data. Note that scanned images of a 1 cm-long bone of a mouse, used as a scale bar, was deleted in order to prevent the mouse bone from concealing the entire skeleton when the image is rotated in the movie.

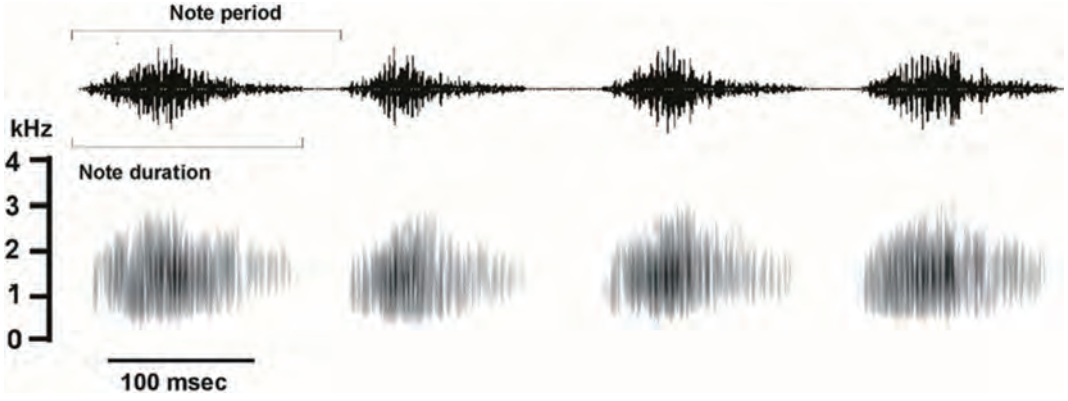

Figure S1 Oscillogram and sound spectrogram of the advertisement call of *Hyla japonica*.

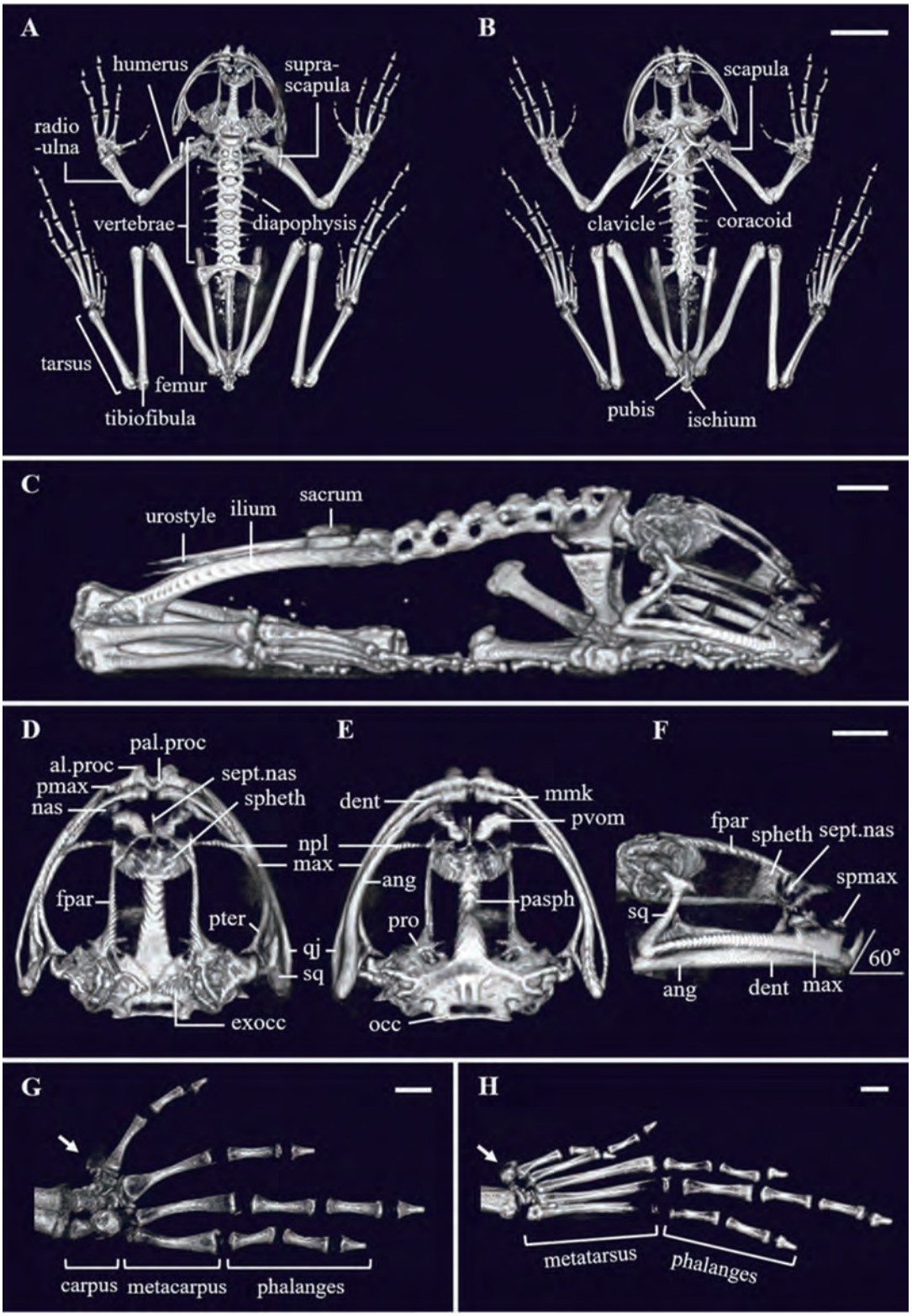

Figure S2 3D micro-CT images of another frog of *Hyla suweonensis*. All images were acquired in the same way as making Figure 3 images and generated via micro-CT viewer and 3D viewer programs both provided by PerkinElmer. Entire skeleton images (A to C) were made from the 4-minuate-long micro-CT scan for the whole body in a high resolution mode (i.e. 0.16 Gy). Images for the skull (D to F) were made from the enlarged entire skeleton images. Images for the manus and pes (G–H) were individually made from a micro-CT scan set-up (FOV: 25 mm × 25 mm, scan time: 4 min, scan mode: high resolution) with the total X-ray dose of 2.95 Gy. The feature of the vertebral column, phalangeal formula, shape of distal end of phalanges, and Emerson's ilio-sacral articulation type shown in this figure are almost identical to those in Figure 3. Scale bars: 5 mm (A–B), 2 mm (C–F), and 1 mm (G–H).